The Apparent Constant-Phase-Element Behavior of a Disk Electrode with Faradaic Reactions

Vicky Mei-Wen Huang, Vincent Vivier, Mark E. Orazem, Nadine Pébère, Bernard Tribollet

The Apparent Constant-Phase-Element Behavior of a Disk Electrode with Faradaic Reactions

A Global and Local Impedance Analysis

Vicky Mei-Wen Huang,[a,*] Vincent Vivier,[b,] Mark E. Orazem,[a,***,z] Nadine Pébère,[c,**] and Bernard Tribollet[b,**]**

[a]*Department of Chemical Engineering, University of Florida, Gainesville, Florida 32611, USA*
[b]*UPR 15 du CNRS, Laboratoire Interfaces et Systèmes Electrochimiques, Université Pierre et Marie Curie, 75252 Paris, France*
[c]*CIRIMAT, UMR CNRS 5085, ENSIACET, 31077 Toulouse Cedex 04, France*

Geometry-induced current and potential distributions modify the global impedance response of a disk electrode subject to faradaic reactions. The problem was treated for both linear and Tafel kinetic regimes. The apparent capacity of a disk electrode embedded in an insulating plane was shown to vary considerably with frequency. At frequencies above the characteristic frequency for the faradaic reaction, the global impedance response has a quasi-constant-phase element (CPE) character, but with a CPE coefficient α that is a function of both dimensionless frequency K and dimensionless current density J. For small values of J, α approached unity, whereas, for larger values of J, α reached values near 0.78. The calculated values of α are typical of those obtained in impedance measurements on disk electrodes. For determining the interfacial capacitance, the influence of current and potential distributions on the impedance response cannot be neglected, even if the apparent CPE exponent α has values close to unity. Several methods taken from the literature were tested to determine their suitability for extracting interfacial capacitance values from impedance data on disk electrodes. The best results were obtained using a formula which accounted for both ohmic and charge-transfer resistances.

[DOI: 10.1149/1.2398894]

The geometry of an electrode frequently constrains the distribution of current density and potential in the electrolyte adjacent to the electrode in such a way that both cannot simultaneously be uniform. The primary and secondary current and potential distributions associated with a disk embedded in an insulating plane have been developed by Newman.[1,2] Newman showed that the potential distribution on the disk electrode is not uniform under conditions where the current density is uniform and, conversely, the current distribution is nonuniform under the primary condition where the solution potential is uniform.[2,3]

The nonuniform current and potential distribution associated with the disk geometry influences the transient and the impedance response. Nisancioglu and Newman[4,5] modeled the transient response of a disk electrode to step changes in current. The solution to Laplace's equation was performed using a transformation to rotational elliptic coordinates and a series expansion in terms of Legendre polynomials. Antohi and Scherson have recently expanded the solution to the transient problem by expanding the number of terms used in the series expansion.[6]

Newman demonstrated that geometry-induced current and potential distributions cause a frequency dispersion that distorts the impedance response of a disk electrode.[7] Nisancioglu showed the extent to which this frequency dispersion causes an error in the values for charge-transfer resistance and interfacial capacitance obtained from impedance data.[8,9] The discussion by Nisancioglu[8,9] and by Newman[7] did not address the common practice of describing nonideal impedance response in terms of constant-phase elements.

The impedance response typically reflects a distribution of reactivity that is commonly represented in equivalent electrical circuits as a constant-phase element (CPE).[10-12] The impedance associated with a simple faradaic reaction without diffusion can be expressed in terms of a CPE as

$$Z(\omega) = R_e + \frac{R_t}{1 + (j\omega)^{\alpha} Q R_t} \qquad [1]$$

where the parameters α and Q are independent of frequency. When $\alpha = 1$, Q has units of a capacitance, i.e., $\mu F/cm^2$, and represents the capacity of the interface. When $\alpha \neq 1$, the system shows behavior that has been attributed to surface heterogeneity[13,14] or to continuously distributed time constants for charge-transfer reactions.[15-19] Independent of the cause of CPE behavior, the phase angle associated with a CPE is independent of frequency.

Huang et al.[20] have shown that current and potential distributions induce a high-frequency pseudo-CPE behavior in the global impedance response of an ideally polarized blocking electrode with a local ideally capacitive behavior. In a related work, Huang et al.[21] explored the role of current and potential distribution on the global and local impedance response of a blocking electrode exhibiting a local CPE behavior. They were able to relate the global impedance response to local impedance, and distinctive features of the calculated global and local impedance response were verified experimentally.

Using both global and local impedance measurements on a magnesium alloy, Jorcin et al.[22] have shown that the geometry of a disk in an insulating plane can induce CPE behavior and that this CPE behavior can be associated with a radial distribution of local resistance. The authors proposed that these results could be explained in terms of the numerical and analytic treatment for the impedance response of a disk electrode presented by Newman[7] and by Nisancioglu.[8,9]

The objective of the present work was to explore the role of current and potential distribution on the global and local impedance response of an electrode exhibiting a faradaic behavior. A second objective was to describe the role of the resulting geometry-induced frequency dispersion in terms of CPE behavior.

Mathematical Development

The mathematical development followed that presented by Newman.[7] The development in terms of rotational elliptic coordinates, i.e.

$$y = r_0 \xi \eta \qquad [2]$$

and

* Electrochemical Society Student Member.
** Electrochemical Society Active Member.
*** Electrochemical Society Fellow.
z E-mail: meo@che.ufl.edu

$$r = r_0\sqrt{(1 + \xi^2)(1 - \eta^2)} \quad [3]$$

was summarized by Huang et al. for blocking electrodes.[20,21] The key difference between the present work and that described by Huang et al.[20,21] was the boundary condition applied at the electrode surface.

The problem was solved for two kinetic regimes. Under linear kinetics, following Newman[7] and Nisancioglu,[8,9] the current density at the electrode surface could be expressed as

$$i = C_0\frac{\partial\,(V - \Phi_0)}{\partial\,t} + \frac{(\alpha_a + \alpha_c)i_0F}{RT}(V - \Phi_0) = -\kappa\frac{\partial\,\Phi}{\partial\,y}\bigg|_{y=0}$$
$$= -\frac{\kappa}{r_0\eta}\frac{\partial\,\Phi}{\partial\,\xi}\bigg|_{\xi=0} \quad [4]$$

The assumption of linear kinetics applies for $\bar{i} \ll i_0$. Under the assumption of Tafel kinetics, the current density at the electrode surface could be expressed as

$$i = C_0\frac{\partial\,(V - \Phi_0)}{\partial\,t} - i_0\exp\left(-\frac{\alpha_cF}{RT}(V - \Phi_0)\right) = -\kappa\frac{\partial\,\Phi}{\partial\,y}\bigg|_{y=0}$$
$$= -\frac{\kappa}{r_0\eta}\frac{\partial\,\Phi}{\partial\,\xi}\bigg|_{\xi=0} \quad [5]$$

where the current in the Tafel regime was assumed to be cathodic. A similar expression can be developed under assumption of anodic currents. The results presented here are general because the impedance results do not depend on whether the current is anodic or cathodic.

The flux boundary conditions 4 or 5 apply at the electrode surface ($\xi = 0$). The boundary conditions 4 or 5 were written in frequency-domain as

$$K\tilde{\Phi}_{0,j} + J(\tilde{V}_r - \tilde{\Phi}_{0,r}) = -\frac{1}{\eta}\frac{\partial\,\tilde{\Phi}_r}{\partial\,\xi}\bigg|_{\xi=0} \quad [6]$$

and

$$K(\tilde{V}_r - \tilde{\Phi}_{0,r}) + J\tilde{\Phi}_{0,j} = -\frac{1}{\eta}\frac{\partial\,\tilde{\Phi}_j}{\partial\,\xi}\bigg|_{\xi=0} \quad [7]$$

for linear and Tafel kinetics, respectively. Here, $\tilde{V}_r$ represents the imposed perturbation in the electrode potential referenced to an electrode at infinity, and K is the dimensionless frequency

$$K = \frac{\omega C_0 r_0}{\kappa} \quad [8]$$

Under the assumption of linear kinetics, valid for $\bar{i} \ll i_0$, the parameter J was defined to be

$$J = \frac{(\alpha_a + \alpha_c)Fi_0r_0}{RT\kappa} \quad [9]$$

For Tafel kinetics, valid for $\bar{i} \gg i_0$, the parameter J was defined to be a function of radial position on the electrode surface as

$$J(\eta) = \frac{\alpha_cF|\bar{i}(\eta)|r_0}{RT\kappa} \quad [10]$$

where $\bar{i}(\eta)$ was obtained from the steady-state solution as

$$\bar{i}(\eta) = -i_0\exp\left\{-\frac{\alpha_cF}{RT}[\bar{V}\bar{\Phi}_0(\eta)]\right\} \quad [11]$$

The local charge-transfer resistance for linear kinetics can be expressed in terms of parameters used in Eq. 9 as

$$R_t = \frac{RT}{i_0F(\alpha_a + \alpha_c)} \quad [12]$$

The local charge-transfer resistance for Tafel kinetics can be expressed in terms of parameters used in Eq. 11 as

$$R_t = \frac{RT}{\bar{i}(\eta)\alpha_cF} \quad [13]$$

For linear kinetics, R_t was independent of radial position, but under Tafel kinetics, as shown in Eq. 13, R_t depended on radial position. From a mathematical perspective, the principal difference between the linear and Tafel cases was that J and R_t were held constant for the linear polarization, whereas for the Tafel kinetics, J and R_t were functions of radial position determined by solution of the nonlinear steady-state problem.

The relationship between the parameter J and the charge-transfer and ohmic resistances can be established using the high-frequency limit for the ohmic resistance to a disk electrode obtained by Newman,[1] i.e.

$$R_e = \frac{\pi r_0}{4\kappa} \quad [14]$$

where R_e has units of $\Omega\ \text{cm}^2$. The parameter J can therefore be expressed in terms of the ohmic resistance R_e and charge-transfer resistance R_t as

$$J = \frac{4}{\pi}\frac{R_e}{R_t} \quad [15]$$

Large values of J are seen when the ohmic resistance is much larger than the charge-transfer resistance, and small values of J are seen when the charge-transfer resistance dominates.

The resulting set of equations were solved under the assumption of a uniform capacitance C_0 using the collocation package PDE2D developed by Sewell.[23] Calculations were performed for differing domain sizes, and the results reported here were obtained by extrapolation to an infinite domain size.

Results and Discussion

In a previous article in this series, Huang et al.[20] presented a notation that addressed the concepts of a global impedance, which involved quantities averaged over the electrode surface; a local interfacial impedance, which involved both a local current density and the local potential drop $\tilde{V} - \tilde{\Phi}_0(r)$ across the diffuse double layer; a local impedance, which involved a local current density and the potential of the electrode $\tilde{V}$ referenced to a distant electrode, and a local ohmic impedance, which involved a local current density and potential drop $\tilde{\Phi}_0(r)$ from the outer region of the diffuse double layer to the distant electrode. The corresponding list of symbols is provided in Table I of Huang et al.[20]

The local impedance z can be represented by the sum of local interfacial impedance z_0 and local ohmic impedance z_e as

$$z = z_0 + z_e \quad [16]$$

Huang et al.[20,21] demonstrated for blocking disk electrodes that, while the local interfacial impedance represents the behavior of the system unaffected by the current and potential distributions along the surface of the electrode, the local impedance shows significant frequency dispersion. The local and global ohmic impedances were shown to contain the influence of the current and potential distributions.

While the calculations presented here were performed in terms of solutions of Laplace's equation for a disk geometry, the nature of the electrode–electrolyte interface can be understood in the context of the schematic representation given in Fig. 1. Under linear kinetics, both C_0 and R_t were independent of radial position, whereas for Tafel kinetics, $1/R_t$ varied with radial position in accordance with the current distribution presented in Fig. 2.

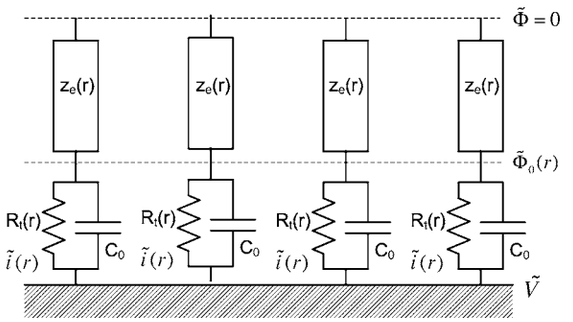

Figure 1. Schematic representation of an impedance distribution for a disk electrode where z_e represents the local ohmic impedance, C_0 represents the interfacial capacitance, and R_t represents the charge-transfer resistance.

The calculated results for global impedance, local impedance, local interfacial impedance, and both local and global ohmic impedances are presented in this section.

Global impedance.— The calculated global impedance response is presented in Fig. 3a for $J = 0.1$ and in Fig. 3b for $J = 1.0$ with dimensionless frequency K as a parameter. The real and imaginary components are presented in dimensionless form. The impedance results for linear kinetics at $J = 0.1$ match closely the impedance response

$$\frac{Z\kappa}{\pi r_0} = \frac{1}{4} + \frac{1}{\pi}\frac{1/J}{1 + jK/J} \qquad [17]$$

calculated in terms of the dimensionless groups used in the present work in the absence of frequency dispersion associated with the geometry-induced current and potential distributions. The impedance response for Tafel kinetics differs because the charge-transfer resistance is a function of radial position. The comparison between the impedance for linear kinetics and Eq. 17 for $J = 1$ shows the distortion of the high-frequency impedance response associated with the influence of current and potential distributions.

The calculated results for linear kinetics in Fig. 3 show good agreement to the corresponding numerical values obtained by Newman.[7] The comparison with Newman's calculations is seen more clearly in the representation of the real and imaginary parts of the impedance response shown in Fig. 4a and 4b, respectively. At low frequencies, values for the real part of the impedance differ for

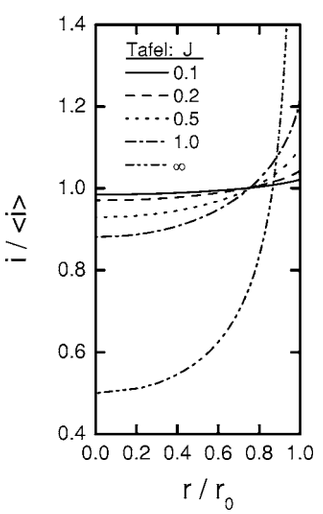

Figure 2. Secondary current distribution for Tafel polarization at a disk electrode with J as a parameter.

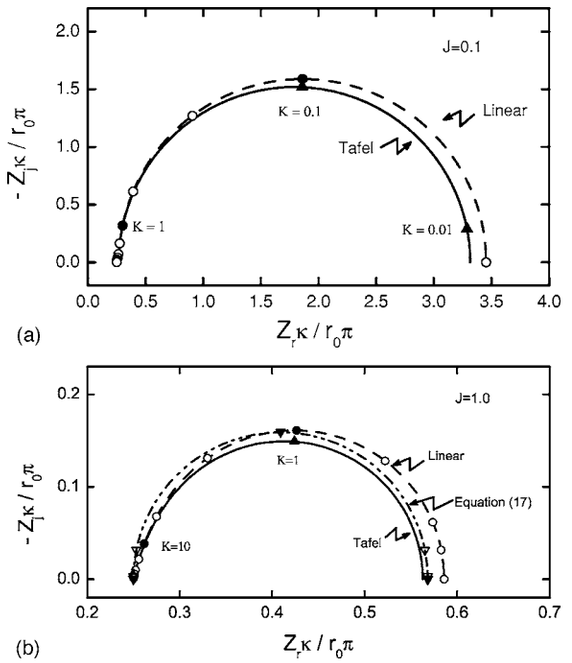

Figure 3. Calculated Nyquist representation of the impedance response for a disk electrode under assumptions of (solid lines) Tafel and (dashed lines) linear kinetics. Open circles represent the result calculated by Newman.[7] (a) $J = 0.1$ and (b) $J = 1.0$.

impedance calculated under the assumptions of linear and Tafel kinetics, whereas the values of the imaginary impedance calculated under the assumptions of linear and Tafel kinetics are superposed for all frequencies. The slope of the lines presented in Fig. 4b are equal to +1 at low frequencies but differ from −1 at high frequencies. The slope of these lines in the high-frequency range can be related to the exponent α used in models for CPE behavior.[24]

The calculated derivative of $\log(Z_j\kappa/r_0\pi)$ with respect to $\log(K)$ (taken from Fig. 4b) is presented in Fig. 5a as a function of K with J as a parameter. At large frequencies, the quantity $d\log(Z_j\kappa/r_0\pi)/d\log(K)$ can be considered to be equal to $-\alpha$ where α is the exponent used for models of CPE behavior. The characteristic frequency where the value of slope deviates from unity increases with the dimensionless parameter J. The transition frequencies correspond to the inverse of the R_tC_0 time constant and, as seen in Fig. 5b, overlap when given as a function of

$$\frac{K}{J} = \frac{\omega C_0 RT}{\bar{i}\alpha_c F} = \omega R_t C_0 \qquad [18]$$

The characteristic frequency for the change in slope is at $K/J = 1$, i.e., at the frequency $\omega_{max} = 1/R_tC_0$. The functional dependence of $d\log(Z_j\kappa/r_0\pi)/d\log(K)$ was independent of assumption of either linear or Tafel kinetics.

Two characteristic frequencies are, therefore, evident in Fig. 5. The characteristic frequency $K/J = 1$ is associated with the R_tC_0 time constant for the faradaic reaction, and the characteristic frequency for the influence of current and potential distributions $K = 1$ is associated with the capacitance C_0 and the ohmic resistance given as Eq. 14.

Local interfacial impedance.— The calculated local interfacial impedance for Tafel kinetics with $J = 1$ is presented in Fig. 6 as a function of frequency with normalized radial position on the disk r/r_0 as a parameter. At low frequencies, the local interfacial impedance, for both real and imaginary, is smallest at the periphery and

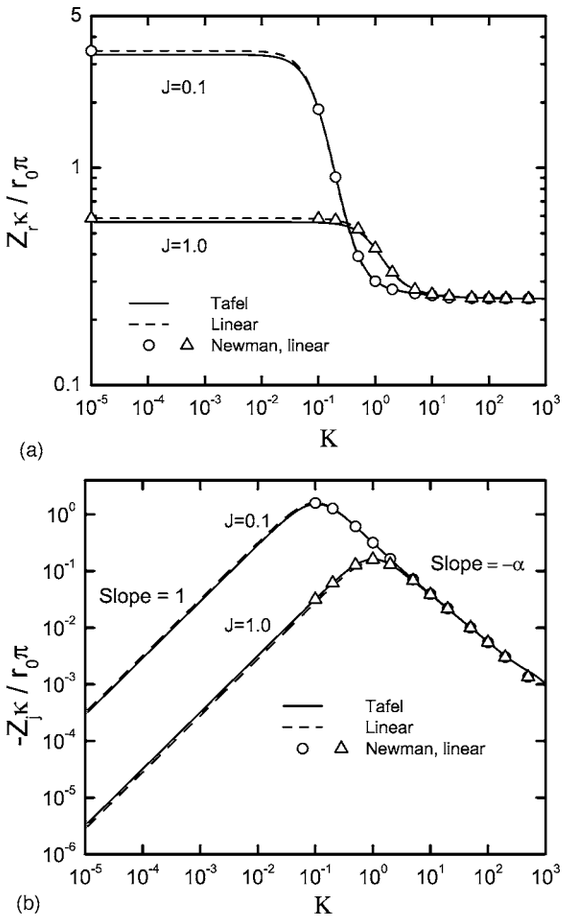

Figure 4. Calculated representation of the impedance response for a disk electrode under assumptions of Tafel and linear kinetics and with J as a parameter. Open symbols represent the result calculated by Newman:[7] (a) real part and (b) imaginary part.

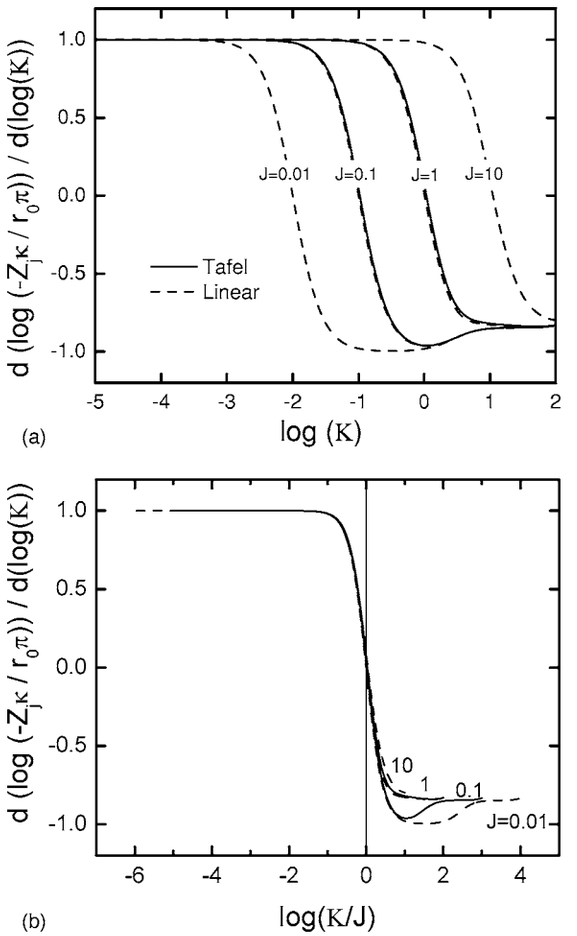

Figure 5. The calculated derivative of $\log(Z_j\kappa/r_0\pi)$ with respect to $\log(K)$ (taken from Fig. 4b) with J as a parameter: (a) as a function of K and (b) as a function of K/J (see Eq. 18).

largest at the center of the disk. The variation at low frequencies is less distinguishable for smaller values of J. All the curves in Fig. 6a and b are superposed at frequencies $K > 1$.

For the linear kinetics calculation, where J is independent of radial position, the scaled real part of the local interfacial impedance follows

$$\frac{z_{0,r}\kappa}{r_0\pi} = \frac{J}{\pi(J^2 + K^2)} \qquad [19]$$

and the imaginary part of the local interfacial impedance follows

$$\frac{z_{0,j}\kappa}{r_0\pi} = \frac{-K}{\pi(J^2 + K^2)} \qquad [20]$$

Plots similar to Fig. 7 were obtained for the local interfacial impedance calculated under the assumption of linear kinetics, but for linear kinetics the local interfacial impedance was independent of radial position.

The local interfacial impedance for Tafel kinetics with $J = 1$ is presented in Fig. 7 as a function of normalized radial position with frequency as a parameter. The lines for $K = 0.01$ and $K = 100$ are superposed in both real and imaginary parts of the local interfacial impedance (Fig. 7a and b, respectively). The real part of the impedance, presented in Fig. 7a, shows a distribution at low frequencies due to the variation of the steady-state current density. Under the Tafel kinetics assumption that J is a function of radial position, as shown in Fig. 7, the real and imaginary parts of the local interfacial impedance change around the values given in Eq. 19 and 20 and have minimum values at the periphery of the disk.

Local impedance.— The calculated local impedance for Tafel and linear kinetics with $J = 1$ is presented in Fig. 8 in Nyquist format with radial position as a parameter. In both cases, the impedance is largest at the center of the disk and smallest at the periphery, reflecting the greater accessibility of the periphery of the disk electrode. Similar results were also obtained for $J = 0.1$, but the differences between radial positions were much less significant. Inductive loops are observed at high frequencies and these are seen in both Tafel and linear calculations for $J = 0.1$ and $J = 1.0$.

The real and imaginary parts of the local impedance for Tafel kinetics with $J = 1.0$ are presented in Fig. 9a and b, respectively. The real part of the local impedance presented in Fig. 9a reaches asymptotic values at $K \to 0$ and $K \to 100$. The absolute value of the imaginary part presented in Fig. 9b shows the change of sign associated with the inductive features seen in Fig. 8a. The changes in sign occur at frequencies below $K = 100$, indicating that the inductive loop cannot be attributed to calculation artifacts.

Local ohmic impedance.— The local ohmic impedance z_e accounts for the difference between the local interfacial and the local impedances. The calculated local ohmic impedance for Tafel kinetics with $J = 1.0$ are presented in Fig. 10 in Nyquist format with normalized radial position as a parameter. The results obtained here for the local ohmic impedance are very similar to those reported for

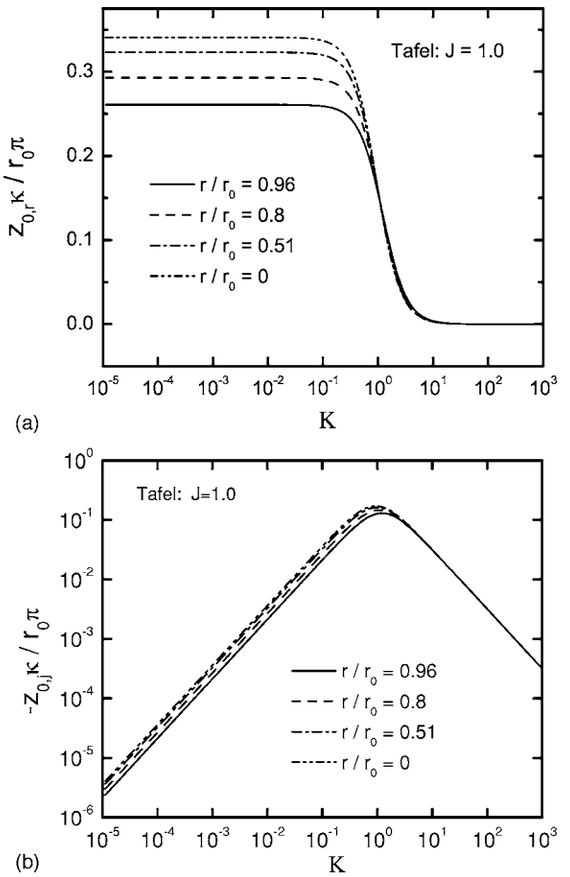

Figure 6. Calculated representation of the local interfacial impedance response for a disk electrode as a function of dimensionless frequency K under assumptions of Tafel kinetics with $J = 1.0$: (a) real part and (b) imaginary part.

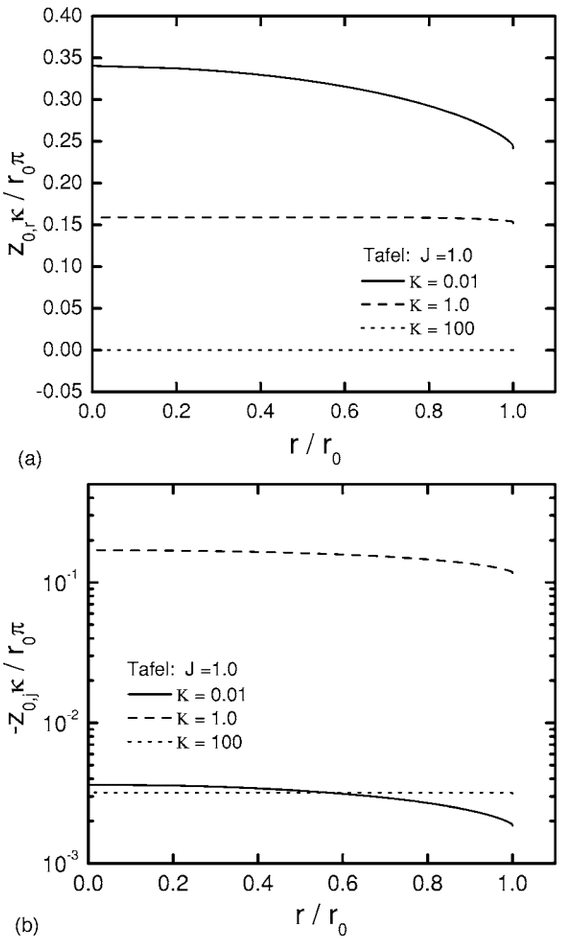

Figure 7. Calculated representation of the local interfacial impedance response for a disk electrode as a function of radial position under assumptions of Tafel kinetics with $J = 1.0$: (a) real part and (b) imaginary part.

the ideally polarized electrode and for the blocking electrode with local CPE behavior.[20,21] At the periphery of the electrode, two time constants (inductive and capacitive loops) are seen, whereas at the electrode center only an inductive loop is evident. These loops are distributed around the asymptotic real value of 1/4.

The calculated values for real and imaginary parts of the local ohmic impedance are presented in Fig. 11a and b, respectively, as a function of frequency with radial position as a parameter. The local ohmic impedance has only real values at $K \to 0$ and $K \to \infty$, but in the frequency range $10^{-2} < K < 100$, z_e has both real and imaginary components. This range of dimensionless frequency was not dependent on the value of J. The local ohmic impedance obtained for linear kinetics and for different J were similar to the results reported here for $J = 1$.

The representation of an ohmic impedance as a complex number represents a departure from standard practice, and the related insights constitute a major contribution of the present work. As shown in previous sections, the local impedance has inductive features that are not seen in the local interfacial impedance. These inductive features are implicit in the local ohmic impedance. As similar results were obtained for ideally polarized[20] and blocking electrodes with local CPE behavior,[21] the result cannot be attributed to faradaic reactions and can be attributed only to the ohmic contribution of the electrolyte.

Global interfacial and global ohmic impedance.— The global interfacial impedance for linear kinetics is independent of radial position and is given by

$$Z_0 = \frac{R_t}{1 + j\omega C_0 R_t} \qquad [21]$$

The global ohmic impedance Z_e is obtained from the global impedance Z by the expression

$$Z_e = Z - Z_0 \qquad [22]$$

The real part of Z_e, obtained for linear kinetics, is given in Fig. 12a, and the imaginary part of Z_e is given in Fig. 12b as functions of dimensionless frequency K with J as a parameter. In the low frequency range $Z_e\kappa/r_0\pi$ is a pure resistance with a numerical value that depends weakly on J. All curves converge in the high frequency range such that $Z_e\kappa/r_0\pi$ tends towards 1/4. The imaginary part of the global ohmic impedance shows a nonzero value in the frequency range that is influenced by the current and potential distributions.

At high and low frequency limits, the global ohmic impedance defined in the present work is consistent with the accepted understanding of the ohmic resistance to current flow to a disk electrode. The global ohmic impedance approaches, at high frequencies, the primary resistance for a disk electrode (Eq. 14) described by Newman.[1] This result was obtained as well for ideally polarized[20] and blocking electrodes with local CPE behavior.[21] The global ohmic impedance approaches, at low frequencies, the value for the ohmic resistance calculated by Newman[7] for a disk electrode. Again, this result was seen as well for blocking electrodes.[20,21] The complex nature of both the global and local ohmic impedances is seen at intermediate frequencies. This complex value is the origin of the

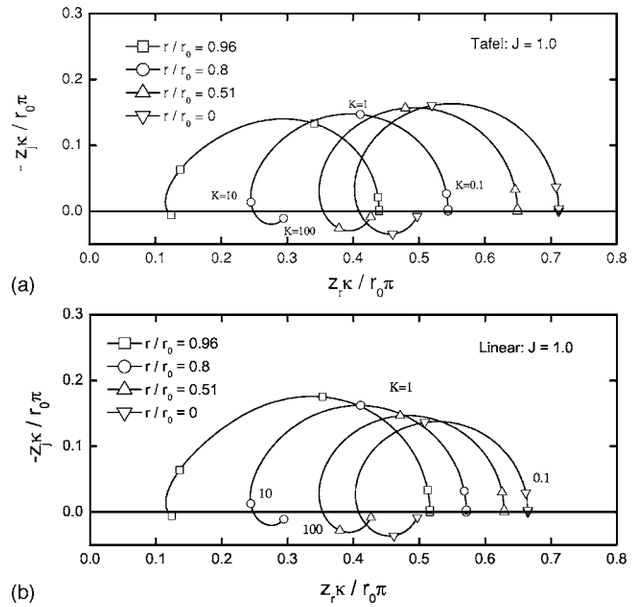

Figure 8. Calculated representation of the local impedance response for a disk electrode as a function of dimensionless frequency K under assumptions of Tafel kinetics with $J = 1.0$: (a) Tafel kinetics and (b) linear kinetics.

inductive features calculated for the local impedance and the quasi-CPE behavior found at high frequency for the global impedance.

Interpretation of Impedance Results

In 1987, Nisancioglu estimated the error caused by frequency dispersion in evaluating physical properties such as charge-transfer resistance and capacitance.[8] A parallel analysis is presented here in terms of the commonly used CPE models.

Determination of charge-transfer resistance.— The impedance response of a disk electrode in the absence of frequency dispersion associated with the geometry-induced current and potential distributions can be expressed by Eq. 17. The corresponding charge-transfer resistance evident at low frequencies is given by

$$\frac{R_t\kappa}{\pi r_0} = \frac{1}{\pi J} \qquad [23]$$

The effective global charge-transfer resistance can be estimated from the calculated impedance data according to

$$\frac{R_{\text{eff}}\kappa}{\pi r_0} = \left.\frac{Z_r\kappa}{\pi r_0}\right|_{K=0} - \frac{1}{4} \qquad [24]$$

The value of R_{eff}/R_t is presented in Fig. 13 as a function of J under the assumption of linear kinetics. The results are in full agreement with those presented in a different format by Nisancioglu.[8] The influence of the frequency dispersion is greatest when J is large, i.e., when the ohmic resistance dominates over the charge-transfer resistance. At $J = 100$, an error of 75% is seen in the estimation of the charge-transfer resistance.

Determination of capacitance.— The evaluation of interfacial capacitance is perhaps better done in terms of the CPE. The values of α and $1 - \alpha$ obtained from Fig. 5a are presented in Fig. 14 as functions of J. The value of α ranges from 0.98 for $J = 0.01$ to 0.87 for $J = 10$, which demonstrates that nonuniform current and potential distributions on a disk electrode can yield high-frequency CPE-like behavior. As J becomes small, i.e., as the charge-transfer resistance dominates over the ohmic resistance, α tends toward unity. It is significant that the calculated value of α shown in Fig. 14 corresponds to a range of α that is frequently observed in experiments.

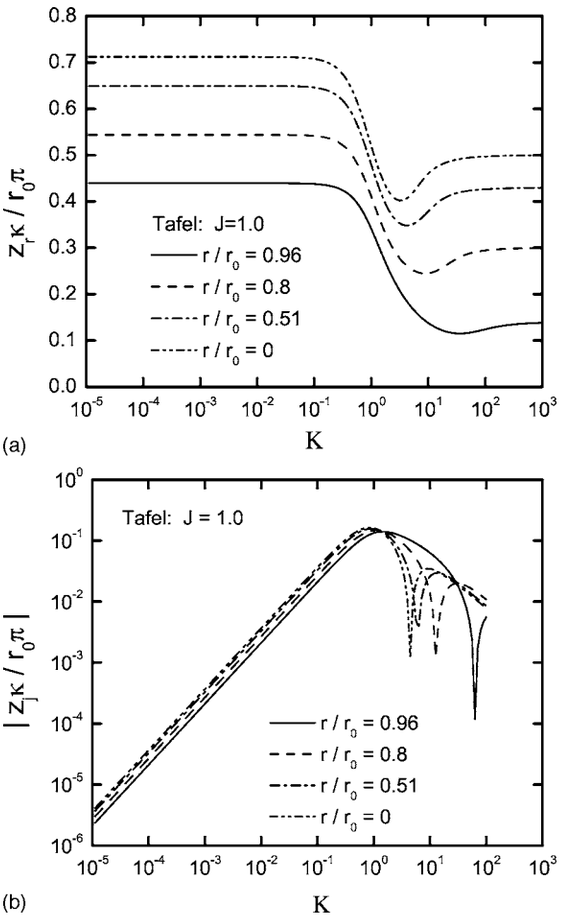

Figure 9. Calculated representation of the local impedance response for a disk electrode as a function of dimensionless frequency K with $J = 1.0$: (a) real part and (b) absolute value of the imaginary part.

The effective CPE coefficient Q_{eff} for electrochemical systems can be obtained from the imaginary part of the impedance as

$$Q_{\text{eff}} = \sin\left(\frac{\alpha\pi}{2}\right)\frac{-1}{Z_j\omega^{\alpha}} \qquad [25]$$

The value of effective CPE coefficient, scaled by the interfacial capacitance, is presented in Fig. 15 as a function of J. The frequencies reported in Fig. 15 are limited to those that are one decade larger than the characteristic frequency ($\omega_{\max}$ or $K/J = 1$) because, in this frequency range, the value of α is well-defined. Figure 15 was developed taking into account the observation, seen in Fig. 5a, that the value of α is dependent on the frequency at which the slope

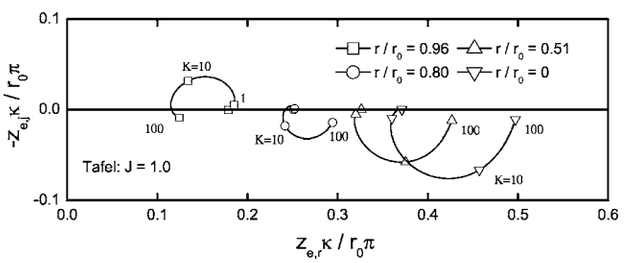

Figure 10. Calculated representation of the local ohmic impedance response for a disk electrode as a function of dimensionless frequency K under assumptions of Tafel kinetics with $J = 1.0$

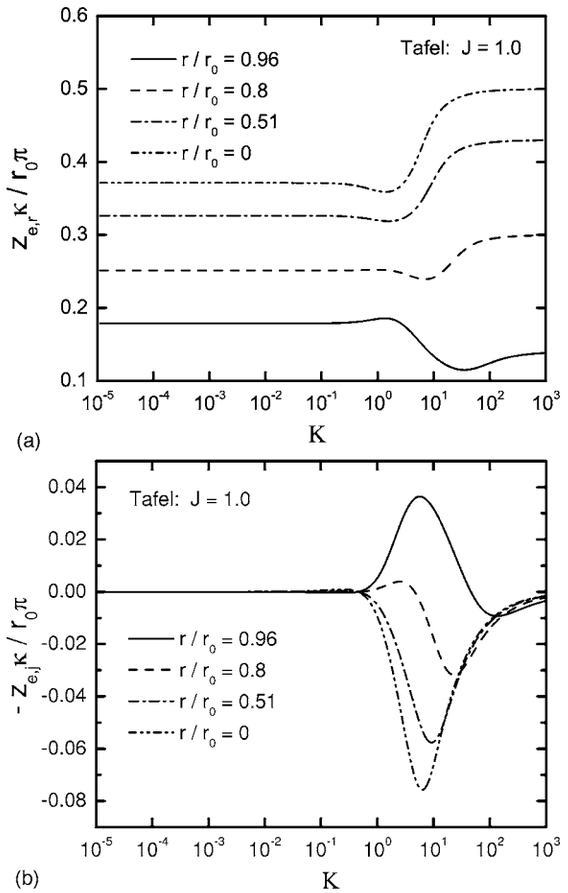

Figure 11. Calculated representation of the local ohmic impedance response for a disk electrode as a function of dimensionless frequency K under assumptions of Tafel kinetics with $J = 1.0$: (a) real part and (b) imaginary part.

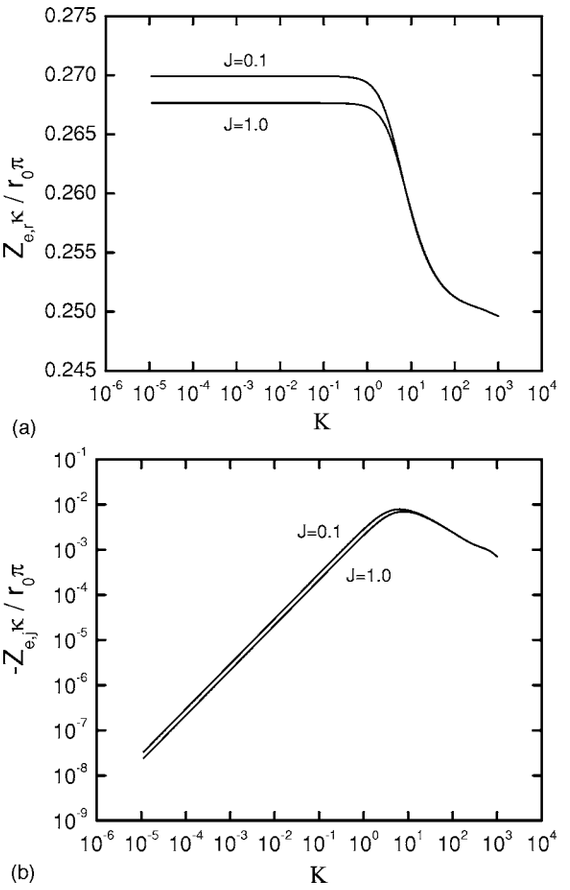

Figure 12. Calculated global ohmic impedance response for a disk electrode as a function of dimensionless frequency for linear kinetics for $J = 0.1$ and $J = 1.0$: (a) real part and (b) imaginary part.

is evaluated. Thus, the value of Q_{eff} reported is that corresponding to the value of α at a given frequency K.

Figure 15 is presented here because, while the dimensions are not exactly that of a capacitance, the CPE coefficient is often assumed to have approximately the same numerical value as the interfacial capacitance. The value of Q_{eff} is a function of frequency. At high frequencies, where frequency dispersion plays a significant role, the effective CPE coefficient Q_{eff} provides an inaccurate estimate for the interfacial capacitance, even for small values of J where α is close to unity. The errors in estimating the interfacial capacitance are on the order of 500% at $K = 100$.

A number of researchers have explored the relationship between CPE parameters and the interfacial capacitance. Hsu and Mansfeld[25] proposed

$$C_{\text{eff}} = Q(\omega_{\max})^{\alpha-1} = Q\left(\frac{\kappa K_{\max}}{C_0 r_0}\right)^{\alpha-1} \qquad [26]$$

where $\omega_{\max}$ (or $K_{\max}$) is the characteristic frequency at which the imaginary part of the impedance reaches its maximum magnitude and C_{eff} is the estimated interfacial capacitance. Equation 26 is tested against the input value of interfacial capacitance in Fig. 16 where C_0 is the known interfacial capacitance which was independent of radial position. As described above, Fig. 16 was developed using local frequency-dependent values of α and Q_{eff}. The frequencies reported in Fig. 16 are limited to those that are one decade larger than the characteristic frequency $\omega_{\max}$. While Eq. 26 represents an improvement as compared to direct use of the CPE coefficient Q_{eff}, the errors in estimating the interfacial capacitance depend on both J and K and range between −70 and +100%.

Brug et al.[10] developed a relationship for a blocking electrode between the interfacial capacitance and the CPE coefficient Q as

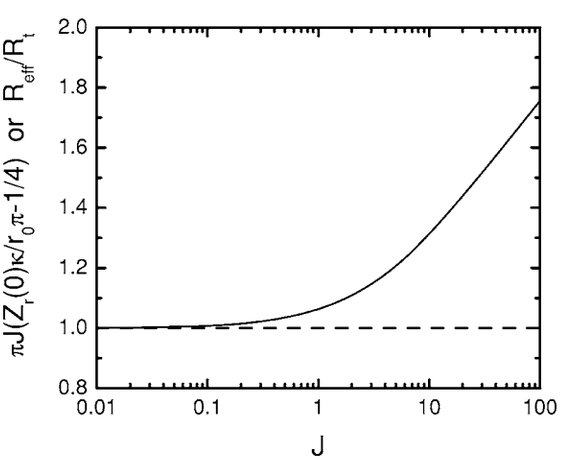

Figure 13. The apparent value of R_{eff}/R_t obtained from the calculated impedance response at low frequencies as a function of J.

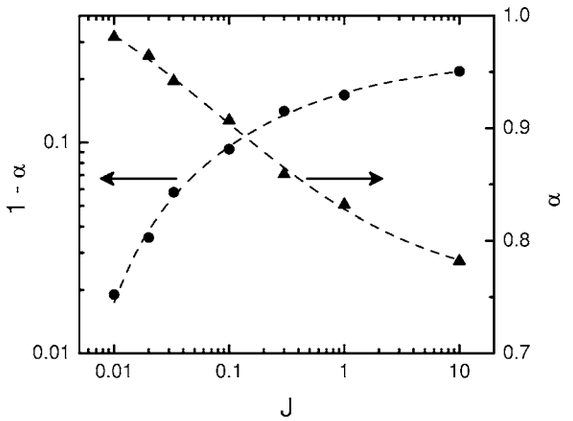

Figure 14. The apparent value of 1 − α obtained from the calculated impedance response at high frequencies as a function of *J*.

$$C_{\text{eff}} = [QR_e^{(1-\alpha)}]^{1/\alpha} \quad [27]$$

A similar relationship between the interfacial capacitance and the CPE coefficient Q was developed for a faradaic system as

$$C_{\text{eff}} = \left[Q\left(\frac{1}{R_e} + \frac{1}{R_t}\right)^{(\alpha-1)} \right]^{1/\alpha} = \left\{ Q\left[\frac{1}{R_e}\left(1 + \frac{\pi J}{4}\right)\right]^{(\alpha-1)} \right\}^{1/\alpha} \quad [28]$$

Equations 27 and 28 are compared to the expected value of interfacial capacitance in Fig. 17a and b, respectively. Figure 17a and b was developed using local frequency-dependent values of α and Q_{eff} over the same frequency range as is reported in Fig. 15 and 16. The frequencies reported in Fig. 17 are limited to those that are one decade larger than the characteristic frequency $\omega_{\max}$. The error in Eq. 27 is a function of both frequency K and J. While Eq. 27 applies strictly for a blocking electrode, it gives the correct answer for faradaic systems if one chooses to calculate α at frequencies $K < 5$ but fails for $K > 5$. The dependence on J is reduced significantly when both the ohmic resistance R_e and charge-transfer resistance R_t are taken into account, and the errors in estimating interfacial capacitance are less than 20%. The correction for R_t in Eq. 28 is important for frequencies $K > 5$. Of the relationships tested, Eq. 28 provides the best means for estimating interfacial capacitance when frequency dispersion is significant.

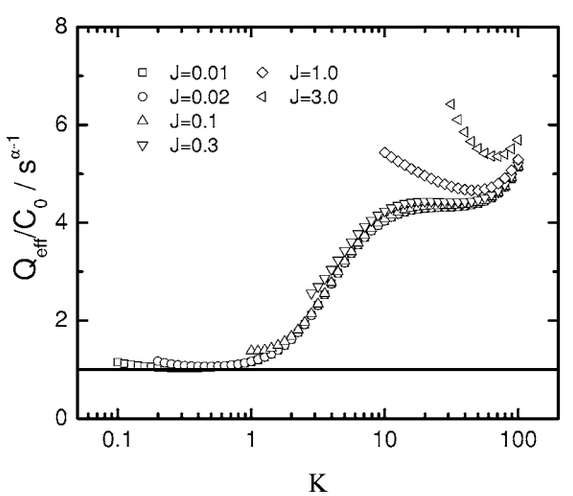

Figure 15. Effective CPE coefficient scaled by the interfacial capacitance as a function of *J*.

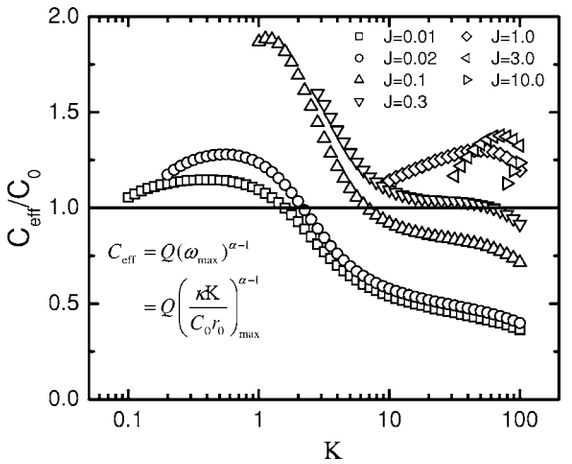

Figure 16. Effective capacitance calculated from Eq. 26 and normalized by the input interfacial capacitance for a disk electrode as a function of dimensionless frequency K with J as a parameter (see Hsu and Mansfeld.[25]).

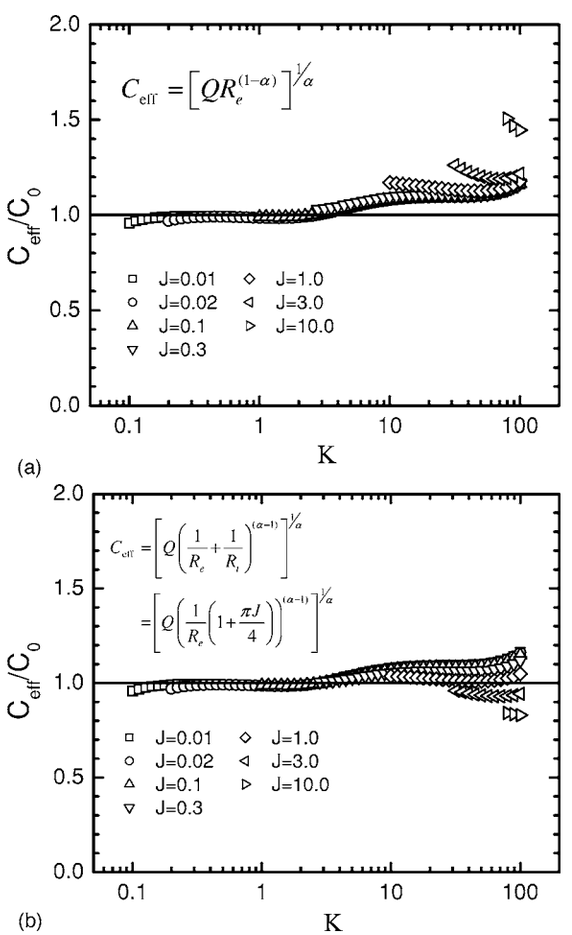

Figure 17. Normalized effective capacitance calculated from relationships presented by Brug et al.[10] for a disk electrode as a function of dimensionless frequency K with J as a parameter: (a) with correction for ohmic resistance R_e (Eq. 27) and (b) with correction for both ohmic resistance R_e and charge-transfer resistance R_t (Eq. 28).

Conclusions

Geometry-induced current and potential distributions modify the global impedance response of a disk electrode subject to faradaic reactions. The calculated local and ohmic impedances are shown to provide insight into the frequency dispersion associated with the geometry of disk electrodes. While the calculated global impedance is purely capacitive, the local impedance has high-frequency inductive loops. The local impedance is influenced by the local ohmic impedance, which has complex behavior near dimensionless frequency $K = 1$. The imaginary part of both the local and global ohmic impedances is equal to zero at both high and low frequencies where the ohmic impedance has purely resistive character.

The results of the present work support the conclusion offered by Newman[7] that the apparent capacity of a disk electrode embedded in an insulating plane varies considerably with frequency. At frequencies above the characteristic frequency for the faradaic reaction, the global impedance response has a quasi-CPE character but with a CPE coefficient α that is a function of both frequency K and dimensionless exchange current density J. For small values of J, α approached unity, whereas for larger values of J, α reached values near 0.78. The calculated values of α are typical of those obtained in impedance measurements on disk electrodes.

Several methods were tested to determine their suitability for extracting interfacial capacitance values from impedance data on disk electrodes. The best results were obtained using the formula (Eq. 28) offered by Brug et al.[10] which accounted for both ohmic and charge-transfer resistances. This work showed that, for determining the interfacial capacitance, the influence of current and potential distributions on the impedance response cannot be neglected, even if the apparent CPE exponent α has values close to unity.

Acknowledgment

The authors gratefully acknowledge the financial support of their home institutions, which facilitated this collaboration.

Centre National de la Recherche Scientifique assisted in meeting the publication costs of this article.

References

1. J. S. Newman, *J. Electrochem. Soc.*, **113**, 501 (1966).
2. J. S. Newman, *J. Electrochem. Soc.*, **113**, 1235 (1966).
3. W. H. Smyrl and J. Newman, *J. Electrochem. Soc.*, **119**, 208 (1972).
4. K. Nisancioglu and J. Newman, *J. Electrochem. Soc.*, **120**, 1339 (1973).
5. K. Nisancioglu and J. Newman, *J. Electrochem. Soc.*, **121**, 523 (1974).
6. P. Antohi and D. A. Scherson, *J. Electrochem. Soc.*, **153**, E17 (2006).
7. J. S. Newman, *J. Electrochem. Soc.*, **117**, 198 (1970).
8. K. Nisancioglu, *Corrosion (Houston)*, **43**, 258 (1987).
9. K. Nisancioglu, in *The Measurement and Correction of Electrolyte Resistance in Electrochemical Tests*, p. 61–77, L. L. Scribner and S. R. Taylor, Editors, STP 1056, ASTM, Philadelphia, PA (1990).
10. G. J. Brug, A. L. G. van den Eeden, M. Sluyters-Rehbach, and J. H. Sluyters, *J. Electroanal. Chem. Interfacial Electrochem.*, **176**, 275 (1984).
11. J. R. Macdonald, *Impedance Spectroscopy: Emphasizing Solid Materials and Systems*, John Wiley & Sons, New York (1987).
12. A. Lasia, in *Modern Aspects of Electrochemistry*, Vol. 32, R. E. White, B. E. Conway, and J. O'M. Bockris, Editors, p. 143, Plenum Press, New York (1999).
13. Z. Lukacs, *J. Electroanal. Chem.*, **432**, 79 (1997).
14. Z. Lukacs, *J. Electroanal. Chem.*, **464**, 68 (1999).
15. J. R. Macdonald, *J. Appl. Phys.*, **58**, 1971 (1985).
16. J. R. Macdonald, *J. Appl. Phys.*, **58**, 1955 (1985).
17. R. L. Hurt and J. R. Macdonald, *Solid State Ionics*, **20**, 111 (1986).
18. J. R. Macdonald, *J. Appl. Phys.*, **62**, R51 (1987).
19. J. R. Macdonald, *J. Electroanal. Chem.*, **378**, 17 (1994).
20. V. M.-W. Huang, V. Vivier, M. E. Orazem, N. Pébère, and B. Tribollet, *J. Electrochem. Soc.*, **154**, C81 (2006).
21. V. M.-W. Huang, V. Vivier, I. Frateur, M. E. Orazem, and B. Tribollet, *J. Electrochem. Soc.*, **154**, C89 (2006).
22. J.-B. Jorcin, M. E. Orazem, N. Pébère, and B. Tribollet, *Electrochim. Acta*, **51**, 1473 (2006).
23. G. Sewell, *The Numerical Solution of Ordinary and Partial Differential Equations*, John Wiley and Sons, New York (2005).
24. M. E. Orazem, N. Pébère, and B. Tribollet, *J. Electrochem. Soc.*, **153**, B129 (2006).
25. C. H. Hsu and F. Mansfeld, *Corrosion (Houston)*, **57**, 747 (2001).